Contributions to Geophysics and Geodesy Vol. 55/4, 2025 (393–418)

# Inversion of Rayleigh wave dispersion curve based on beluga whale optimization algorithm

Fengjun WU[1], Xiaoyu WEI[2], KeRong HE[3], Gang LI[1], XinAi XU[1,*]

[1] School of Mathematics and Information Science, Nanchang Normal University, Nanchang, 330032, China;
e-mails: wfj@ncnu.edu.cn; 562672612@qq.com; jxxxa@ncnu.edu.cn

[2] School of Information Engineering, Jiangxi Vocational College of Finance and Economics, Jiujiang, 332000, China;
e-mail: wxy@jxvc.edu.cn

[3] School of Physics and Electronic Information, Nanchang Normal University, Nanchang, 330032, China;
e-mail: hekerong_ncnu@163.com

**Abstract:** Rayleigh wave exploration is a crucial technique in engineering site investigation for obtaining subsurface stratigraphic information. Inverting its dispersion curve can effectively reveal underground structures. However, traditional global optimization algorithms exhibit significant limitations in dispersion curve inversion, including slow convergence, low accuracy, and a tendency towards premature convergence. These issues hinder the precise interpretation of stratigraphic information and impact the efficiency and reliability of engineering surveys. To address these challenges, this paper introduces a novel global optimization algorithm—Beluga Whale Optimization (BWO)—for Rayleigh wave dispersion curve inversion, aiming to improve inversion effectiveness and enhance performance. BWO achieves optimal solution finding by mimicking beluga whale swimming, predation, and falling behaviours. Compared to other heuristic algorithms, BWO demonstrates favourable performance in solving complex functions, offering superior performance and efficiency while ensuring high solution accuracy, convergence speed, and stability. When testing the theoretical model of BWO applied to dispersion curve inversion, first, four noise-free models were used to verify the feasibility of BWO for dispersion curve inversion; subsequently, 15% random noise was added to the models, demonstrating that BWO has strong anti-interference capability; finally, specific multi-mode dispersion data were used to test that BWO can be applied to multi-order dispersion curve inversion. During the inversion of noise-free, noise-containing, and multi-mode dispersion models, BWO was compared with the Particle Swarm Optimization (PSO) algorithm, which proved that BWO has superior inversion performance and can obtain higher-precision solutions. In

*corresponding author, e-mail: jxxxa@ncnu.edu.cn

doi: 10.31577/congeo.2025.55.4.1

the actual data testing, seismic data from Wyoming, USA, were used to verify BWO's capability in processing actual data. Results from theoretical model tests and analysis of field data indicate that BWO possesses characteristics of speed, high accuracy, stability, and strong practicality, making it effectively applicable for the quantitative interpretation of Rayleigh wave dispersion curves.

**Key words:** Rayleigh wave, dispersion curve inversion, global optimization, beluga whale optimization (BWO)

## 1. Introduction

With the acceleration of urbanization and the advancement of major engineering construction, the geological conditions of engineering sites have become increasingly complex. From the concealed excavation of urban subway tunnels to foundation selection for cross-sea bridges, from stability assessments of underground energy storage facilities to disaster early warning for high-steep slopes, the design and construction of every project highly depend on an accurate understanding of the subsurface stratigraphic structure (*Nong et al., 2024; Zhang et al., 2020; Liu et al., 2024*). For instance, in soft soil foundation treatment projects, failure to accurately obtain the shear-wave velocity and thickness distribution of various soil layers may lead to unreasonable foundation reinforcement designs, potentially causing excessive building settlement. Conversely, in tunnel construction through karst-developed areas, errors in stratigraphic information could even trigger major safety accidents like water or mud inrushes (*Liu et al., 2024*). Against this backdrop, how to efficiently and accurately detect the physical and mechanical parameters of shallow subsurface layers (typically 0–50 metres below the surface) has become a core issue in the field of engineering geological investigation (*Wang et al., 2022*).

Rayleigh wave exploration technology holds an irreplaceable core position in shallow engineering geological surveys due to its unique technical characteristics and application advantages, serving as one of the key technical means for finely characterizing shallow stratigraphic structures and efficiently obtaining physical and mechanical parameters (*Fu et al., 2023a,b*). Compared to traditional techniques like seismic reflection and refraction methods, Rayleigh wave exploration exhibits two significant advantages: Firstly, it offers high-resolution imaging of shallow geological structures,

achieving metre-scale precision capable of effectively identifying thin-layer stratigraphic units only a few metres thick, providing reliable technical support for detailed near-surface structure characterization. Secondly, it possesses strong anti-interference capabilities, allowing the collection of waveform data suitable for analysis even in environments with urban construction site vibrations or high-frequency noise from electromagnetic equipment in industrial areas (*Ai et al., 2025*). These technical advantages have led to its widespread application in engineering practices such as foundation bearing capacity assessment, underground pipeline detection, and subgrade compaction testing. Dispersion curve inversion is the critical step in transforming Rayleigh wave exploration technology into actual stratigraphic information. The dispersion curve describes the correspondence between Rayleigh wave propagation velocity and frequency, with different stratigraphic structures producing unique dispersion characteristics. The inversion process involves calculating subsurface parameters (such as layer thickness, shear-wave velocity, Poisson's ratio, etc.) from measured dispersion curves, and its accuracy directly determines the reliability of the final survey results. It can be said that the quality of dispersion curve inversion bridges the gap between field data acquisition and engineering design decisions. Consequently, developing high-precision and high-efficiency inversion methods remains a research hotspot in this field (*Liu et al., 2018; Zeng et al., 2011; Yang et al., 2023; Lamuraglia et al., 2023; Dal Moro et al., 2018*).

Currently, dispersion curve inversion algorithms are mainly divided into two categories: local optimization algorithms and global optimization algorithms, each with its own strengths and weaknesses applicable to different scenarios (*Fu et al., 2022*). Local optimization algorithms, represented by Least Squares (*Dorman and Ewing, 1962; Gabriels et al., 1987; Pei et al., 1994; Ganji et al., 1998; Song et al., 2003*), Levenberg-Marquardt (L-M) algorithm (*Xia et al., 1999*), and Occam's algorithm (*Ai and Cheng, 2009; Song et al., 2007*), operate by starting from an initial model and iteratively adjusting parameters to minimize the error between theoretical and measured dispersion curves. Early on, these algorithms were widely adopted due to their high computational efficiency—under ideal conditions with low parameter dimensionality and an initial model close to the true subsurface, inversion could be completed within tens of iterations. However, their limitations are prominent: Firstly, they exhibit extreme dependence on the

initial model. If the initial model differs significantly from the true values, the inversion results may be unsatisfactory. Secondly, they are highly prone to getting trapped in local minima. When low-velocity interlayers exist in the subsurface, the parameter space may contain multiple local optima, and local algorithms often stop searching after finding the first "seemingly reasonable" solution. Furthermore, algorithm performance heavily relies on the accuracy of the Jacobian matrix, which describes the influence of parameter changes on the dispersion curve; calculation errors in this matrix can cause oscillation or convergence stagnation in the inversion results (*Dal Moro et al., 2007; Arai and Tokimatsu, 2005*). These shortcomings significantly restrict the application of local optimization algorithms under complex subsurface conditions. The emergence of global optimization algorithms offers new approaches to address these issues. These algorithms do not rely on an initial model but perform a global search within the parameter space by simulating natural phenomena (e.g., biological evolution, physical annealing, swarm foraging). Representative methods include Genetic Algorithms, Simulated Annealing, Particle Swarm Optimization (PSO), etc. (*Shi and Jin, 1995; Yamanaka and Ishida, 1996; Zhang et al., 2000; Martínez et al., 2000; Beaty et al., 2002; Calderón-Macías and Luke, 2007; Pei et al., 2007; Lu et al., 2016; Song et al., 2012; Cai et al., 2018a*). For example, Genetic Algorithms simulate the biological evolutionary process of "selection-crossover-mutation" to maintain population diversity for exploring the global optimum, while Particle Swarm Optimization simulates bird flock foraging behaviour, adjusting search directions through information sharing among individuals. Compared to local algorithms, global algorithms show distinct advantages when dealing with complex subsurface inversion: they can potentially find the global optimum even if the initial model differs greatly from reality. However, these algorithms also have drawbacks: Firstly, high computational cost. To ensure search comprehensiveness, thousands or even tens of thousands of iterations are often required, potentially taking hours for multi-layer subsurface inversion. Secondly, susceptibility to premature convergence. If algorithm parameters are set inappropriately (e.g., crossover probability too high in Genetic Algorithms), population diversity diminishes rapidly, leading to premature termination at a non-optimal solution. These problems limit the application of global optimization algorithms in rapid field engineering surveys.

To address the shortcomings of existing algorithms, this paper applies a novel Beluga Whale Optimization (BWO) algorithm (*Zhong et al., 2022*) to Rayleigh wave dispersion curve inversion, aiming to improve inversion effectiveness and meet engineering survey requirements. The BWO algorithm simulates the foraging and migration behaviours of beluga whales in Arctic waters, balancing local search and global exploration capabilities through strategies like "spiral predation" and "group siege", showing potential for solving high-dimensional, multi-extremum optimization problems. To systematically verify the performance of the BWO algorithm in Rayleigh wave inversion, the research unfolds at three levels: First, construct four theoretical geological models ranging from simple to complex—including one 2-layer homogeneous model (simple) and three 4-layer models with transitional gradient layers. Noise is also added to the models to further evaluate algorithm performance comprehensively. By comparing the deviation of inverted parameters from theoretical values and the standard deviation of multiple inversion results, the feasibility (ability to converge to a reasonable solution), effectiveness (whether inversion error meets engineering requirements), and stability (consistency of multiple inversion results) of BWO for dispersion curve inversion are assessed. Secondly, the classic Particle Swarm Optimization (PSO) algorithm is selected as a benchmark for comparison. Performance differences are quantified across three dimensions: Root Mean Square Error (RMSE) measures inversion accuracy, the convergence iteration process evaluates convergence efficiency, to clarify whether BWO exhibits superior performance. Finally, the BWO algorithm is applied to measured Rayleigh wave data from Wyoming, USA. By comparing inversion results with nearby borehole data, the algorithm's practicality in real-world engineering scenarios is validated. Through this research, we aim to provide a new method characterised by high accuracy and stability for Rayleigh wave dispersion curve inversion, promoting the application of Rayleigh wave exploration technology in complex engineering sites and offering more reliable geological foundations for engineering design and construction.

## 2. Basic principles of BWO

The Beluga Whale Optimization (BWO) algorithm is a heuristic optimiza-

tion algorithm inspired by the swimming, predation, and falling behaviours of beluga whales in the ocean. Compared to other heuristic algorithms, BWO demonstrates considerable competitiveness, particularly excelling in handling large-scale application problems and complex functions, offering superior performance and efficiency. The BWO algorithm primarily consists of three evolutionary phases: Exploration, Exploitation, and Whale Fall, corresponding to the whales' swimming, predation, and falling behaviours, respectively. The algorithm has a simple structure, exhibits good capabilities in both global and local search, and demonstrates excellent performance in solving practical problems. Its mathematical model is described below:

### 2.1. Initialization

The positions of belugas can be regarded as search agents, which randomly generate a number of candidate values in the search space. In dispersion curve inversion, these candidate values refer to the shear wave velocity ($vs$) and formation thickness ($thk$) for inversion.

$$X_j^i = Lb_j + (Ub_j - Lb_j) \times \text{rand}\,, \tag{1}$$

$Lb$ is the lower bound of the candidate value $X$, $Ub$ is the upper bound of $X$, and rand is a random number in (0, 1).

Furthermore, the balance factor $B_f$ controls the adjustment of the exploration and exploitation phases in the BWO.

$$B_f = B_0 \cdot \left(1 - \frac{t}{T_{\max}}\right), \tag{2}$$

where $B_0$ is a random number between (0,1), $t$ represents the current iteration number, and $T_{\max}$ is the maximum number of iterations. When the balance factor $B_f > 0.5$, the population is in the exploration phase, performing swimming behaviour. When $B_f < 0.5$, the population is in the exploitation phase and exhibits predation behaviour.

### 2.2. Exploration phase

The exploration phase of the BWO algorithm simulates the social behaviour of beluga whales swimming in pairs, moving randomly in a synchronised or mirrored manner. The position update is as follows:

$$\begin{cases} x_{i,j}^{t+1} = x_{i,p}^{t} + (x_{r,p}^{t} - x_{i,p}^{t})(1 + r_1)\cdot\sin(2\pi r_2), & j = 2, 4, 6... \\ x_{i,j}^{t+1} = x_{i,p}^{t} + (x_{r,p}^{t} - x_{i,p}^{t})(1 + r_1)\cdot\cos(2\pi r_2), & j = 1, 3, 5... \end{cases} \tag{3}$$

where $x_{i,j}^{t+1}$ represents the position of the individual in the next iteration; $p$ is a random integer within the range [1, $D$], $D$ being the problem dimension; $x_{i,p}^{t}$ represents the value of the $i$-th individual in the $p$-th dimension, $x_{r,p}^{t}$ represents the value of a random individual $r$ in a random dimension $p$ during the current iteration, and $r_1$ and $r_2$ are random numbers.

### 2.3. Exploitation phase

The exploitation phase of the BWO algorithm mimics the predation behaviour of beluga whales, involving coordinated movement and cooperative hunting within the population through information exchange. Simultaneously, the Levy flight strategy is employed during exploitation to enhance the algorithm's convergence capability. Its mathematical model is expressed as:

$$x_i^{t+1} = r_3\cdot x_{\text{best}}^{t} - r_4\cdot x_i^{t} + C_1\cdot L_F\cdot(X_r^{t} - x_i^{t}), \tag{4}$$

$$C_1 = 2\cdot r_4\cdot\left(1 - \frac{t}{T_{\max}}\right), \tag{5}$$

where $r_3$ and $r_4$ are random numbers in (0, 1); $x_i^{t}$ and $x_{\text{best}}^{t}$ represent the positions of a random individual and the best individual, respectively; $C_1$ is a step size control parameter measuring the intensity of the Levy flight. $L_F$ represents the Levy flight function:

$$L_F = 0.05 \times \frac{\mu\cdot\sigma}{|\nu|^{\frac{1}{\beta}}} \tag{6}$$

$$\sigma = \left(\frac{\Gamma(1+\beta)\times\sin\left(\pi\cdot\frac{\beta}{2}\right)}{\Gamma\left(\frac{1+\beta}{2}\right)\times\beta\times 2^{\frac{\beta-1}{2}}}\right)^{\frac{1}{\beta}}, \quad \Gamma(x) = (x-1)!, \tag{7}$$

where $u, v \sim$ N(0,1) are random numbers following a normal distribution with mean 0 and variance 1, and $\beta$ is a constant set to 1.5.

### 2.4. Whale fall phase

The whale fall phase of the BWO algorithm mimics the behaviour of beluga whales falling to the ocean floor after death. The population enters the

whale fall phase when the balance factor $B_f \leq W_f$. Belugas are susceptible to external harm during migration and foraging, leading to death and sinking. To maintain constant population size, the whale fall position update formula utilises the individual's current position and the whale fall step size:

$$x_i^{t+1} = r_5 \cdot x_i^t - r_6 \cdot x_r^t + r_7 \cdot x_{\text{step}}^t \,, \tag{8}$$

$$x_{\text{step}}^t = e^{\frac{-C_2 \cdot t}{T}} \cdot (Ub - Lb) \,, \tag{9}$$

$$C_2 = 2W_f \times N \,, \tag{10}$$

$$W_f = 0.1 - 0.05 \cdot \frac{t}{T_{\max}} \,, \tag{11}$$

where $r_5$, $r_6$, and $r_7$ are random numbers between 0 and 1; $Ub$ and $Lb$ are the upper and lower bounds of the optimization problem, respectively; $x_{\text{step}}^t$ represents the whale fall step size; $C_2$ represents a step factor; $W_f$ represents the whale fall probability for a beluga individual. Figure 1 shows the flowchart of the BWO algorithm.

## 3. Theoretical model testing

In engineering practice, the fundamental mode dispersion curve, due to its stronger energy and easier observability, is the primary source of information in collected data. Accordingly, inversion work typically targets the fundamental mode dispersion curve (*Yang et al., 2019*). However, considering the possible presence of higher-mode dispersion phenomena, this paper also tested the case of joint inversion using both fundamental and higher-mode dispersion curves. Among subsurface parameters, shear-wave velocity ($Vs$) and layer thickness ($h$) are the most significant factors influencing changes in Rayleigh wave dispersion curve characteristics; the influence of other parameters is relatively limited (*Fu et al., 2023a,b*). To reduce computational load, this paper only uses $Vs$ and $h$ as evaluation indices for the inversion algorithm; other parameters are determined based on prior information. Given the complexity of real subsurface conditions, the search range for model parameters was set to 50% of the true model values.

Regarding algorithm parameter settings, for BWO, population size and iteration count are key parameters affecting its performance. Therefore, the population size for BWO was set to 30, and the iteration count was set to

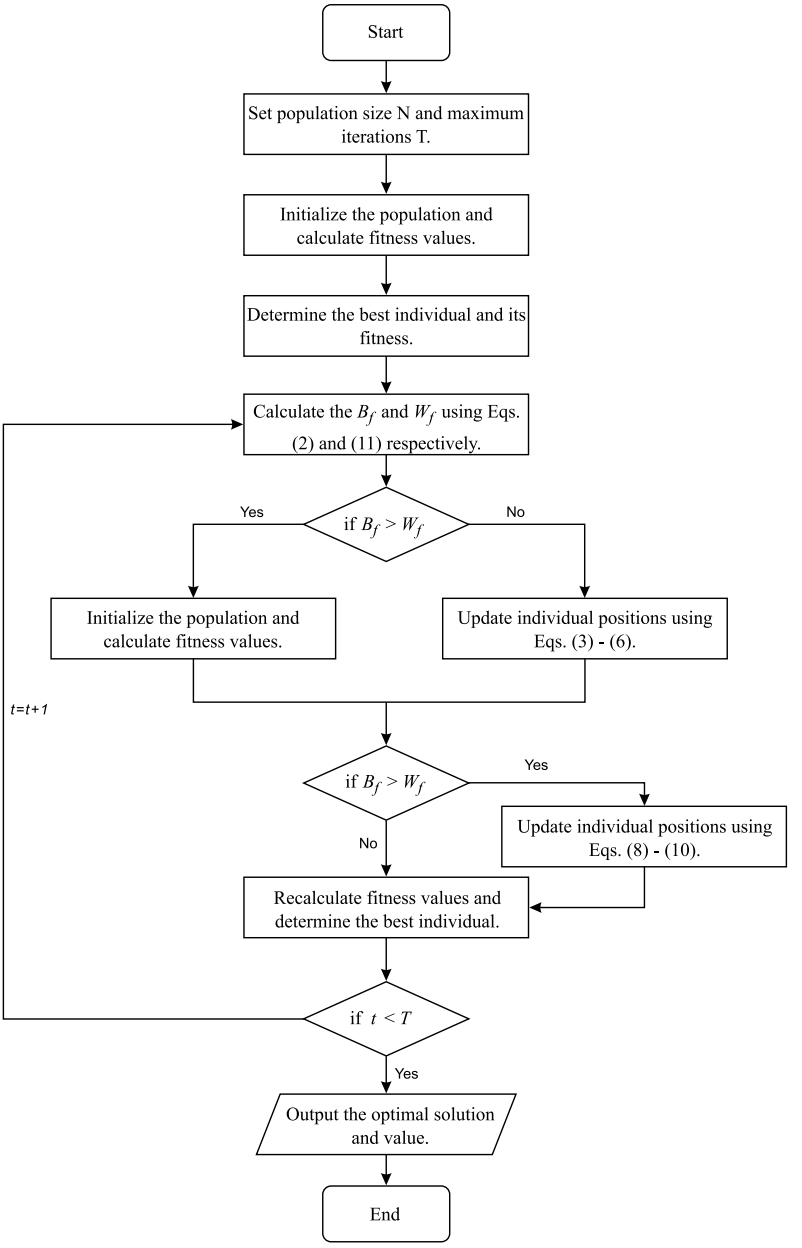


Fig. 1. Flowchart of the BWO algorithm.

100 (*Fu et al., 2023a,b*). To mitigate the effects of algorithm randomness, 10 independent inversions were performed for each theoretical model test, with a different initial model used for each inversion. Finally, the mean of the data obtained from the 10 inversions was taken as the inversion result, while the standard deviation was used as an indicator of algorithm stability for evaluation.

The essence of Rayleigh wave dispersion curve inversion is an optimization problem of minimizing a fitness function. The fitness function adopted in this paper is defined based on the ability of the inverted model to accurately explain the observed data:

$$F = \sqrt{\frac{1}{M}\left\{\sum_{i=1}^{M}\left[v_R^{obs}(i) - v_R^{cal}(i)\right]^2\right\}}, \tag{12}$$

$$G = \frac{1}{L}\sum_{k=1}^{L}\sqrt{\frac{\sum_{i=1}^{M_k}\left(v_R^{obs} - v_R^{cal}\right)^2}{M_k}}. \tag{13}$$

In Eqs. (12) and (13): $v_R^{obs}$ is the measured Rayleigh wave phase velocity; $v_R^{cal}$ is the theoretically calculated Rayleigh wave phase velocity; $M$ is the number of frequency points; $L$ is the number of dispersion curves; $M_k$ is the number of frequency points for the $k$-th dispersion curve.

To reasonably evaluate the performance of the BWO algorithm, this paper selected four theoretical models commonly used in engineering surveys for testing. These four models range from simple to complex, gradually increasing in complexity and approaching real subsurface conditions. Model parameters are detailed in Table 1. Among them, model A is a two-layer velocity-increasing model, model B is a four-layer velocity-increasing model, model C is a four-layer model containing one low-velocity soft interlayer, and model D is a four-layer model containing one high-velocity hard interlayer.

### 3.1. Inversion of noise-free data

To thoroughly evaluate algorithm performance, testing progressed from a basic two-layer model to complex four-layer models, increasing model complexity. Observing the inversion results for the simple two-layer velocity-increasing model (model A) in Figure 2 reveals: even without prior information, the inverted dispersion curve (dotted line in a) maintains a high degree

of fit with the theoretically simulated dispersion curve (solid line in a). The dispersion curves and S-wave velocity models inverted by BWO are both closer to the true values than those obtained by PSO. The parameter errors between the BWO inverted model and the theoretical model are only 0.38%, 0.58%, and 5.80% (detailed in Table 2). Simultaneously, the standard deviations of parameters obtained from 10 independent inversions show low overall deviation across multiple runs, with the maximum deviation being only 5.98. The above results confirm that the BWO algorithm is feasible and stable for dispersion-curve inversion in simple layered structures and outperforms the PSO algorithm on the two-layer model.

Table 1. Model parameters and search space.

| Model | Layers | Model Parameters | | | | Search Range | |
|---|---|---|---|---|---|---|---|
| | | $Vs$ (m/s) | $Vp$ (m/s) | $\rho$ (g/cm$^3$) | $h$ (m) | $Vs$ (m/s) | $h$ (m) |
| A | 1 | 200 | 566 | 2 | 5 | 100 ∼ 300 | 2.5 ∼ 7.5 |
| | 2 | 450 | 900 | 2 | ∞ | 225 ∼ 675 | ∞ |
| B | 1 | 200 | 566 | 2 | 2 | 100 ∼ 300 | 1 ∼ 3 |
| | 2 | 320 | 727 | 2 | 3 | 160 ∼ 480 | 1.5 ∼ 4.5 |
| | 3 | 460 | 913 | 2 | 5 | 230 ∼ 690 | 2.5 ∼ 7.5 |
| | 4 | 530 | 1006 | 2 | ∞ | 265 ∼ 795 | ∞ |
| C | 1 | 200 | 566 | 2 | 3 | 100 ∼ 300 | 1.5 ∼ 4.5 |
| | 2 | 150 | 500 | 2 | 2 | 75 ∼ 225 | 1 ∼ 3 |
| | 3 | 360 | 780 | 2 | 6 | 180 ∼ 540 | 3 ∼ 9 |
| | 4 | 480 | 940 | 2 | ∞ | 240 ∼ 720 | ∞ |
| D | 1 | 150 | 500 | 2 | 4 | 75 ∼ 225 | 2 ∼ 6 |
| | 2 | 300 | 700 | 2 | 4 | 150 ∼ 450 | 2 ∼ 6 |
| | 3 | 240 | 620 | 2 | 5 | 120 ∼ 360 | 2.5 ∼ 7.5 |
| | 4 | 600 | 1100 | 2 | ∞ | 300 ∼ 900 | ∞ |

To further validate the inversion capability of BWO under complex stratigraphic conditions and compare its performance with PSO, inversion experiments were continued on three types of complex formations—models B, C, and D—to test the performance of both algorithms. The test results are detailed in Figure 3, where subfigures a-f correspond to the inversion effectiveness of models B, C, and D, respectively. Analysis of the inversion data shows that for all model types, the dispersion curves generated by

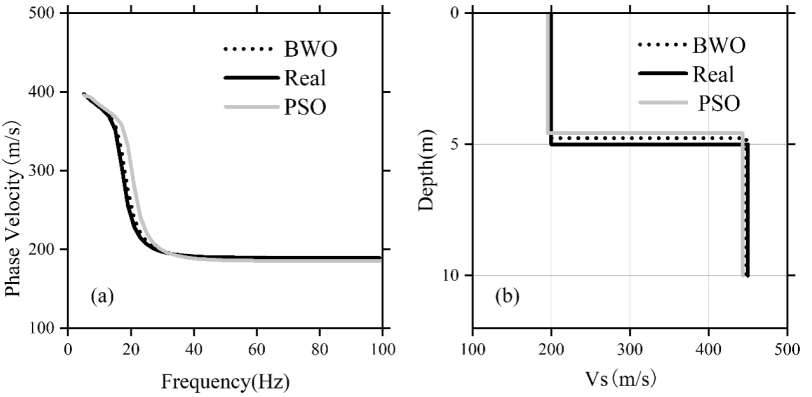


Fig. 2. Inversion results for model A: (a) inverted dispersion curve; (b) inverted shear-wave velocity profile.

BWO inversion (dotted lines in a, c, e) exhibit high consistency with the theoretical dispersion curves (solid lines in a, c, e). The dispersion curves inverted by PSO (gray solid lines in a, c, e) also agree well with the theoretical ones. In terms of parameter inversion, the maximum relative error yielded by BWO is only 7.67%, and the standard deviation remains low, with a maximum value of 13.58. In contrast, PSO produces a maximum relative error of 10.25% and a maximum standard deviation of 28.71 (see Tables 2 and 3). This fully demonstrates that even when facing dispersion curve inversion tasks for complex subsurface models, BWO can maintain good performance, and its inversion performance still outperforms PSO.

### 3.2. Inversion of noise-contaminated data

The presence of noise is unavoidable during seismic data acquisition. Such noise causes small-scale random fluctuations in the extracted dispersion curves, thereby interfering with inversion results. Therefore, before applying an algorithm to real data processing, it is necessary to test its noise resistance. To evaluate BWO's anti-noise performance, 15% random noise was added to the dispersion curves obtained from forward modelling of the aforementioned four theoretical models, followed by inversion.

The noise addition method used in the article is as follows:

$$v_{\text{noise}} = v[1 + 2\,(0.5 - r)\,p]\,. \tag{14}$$

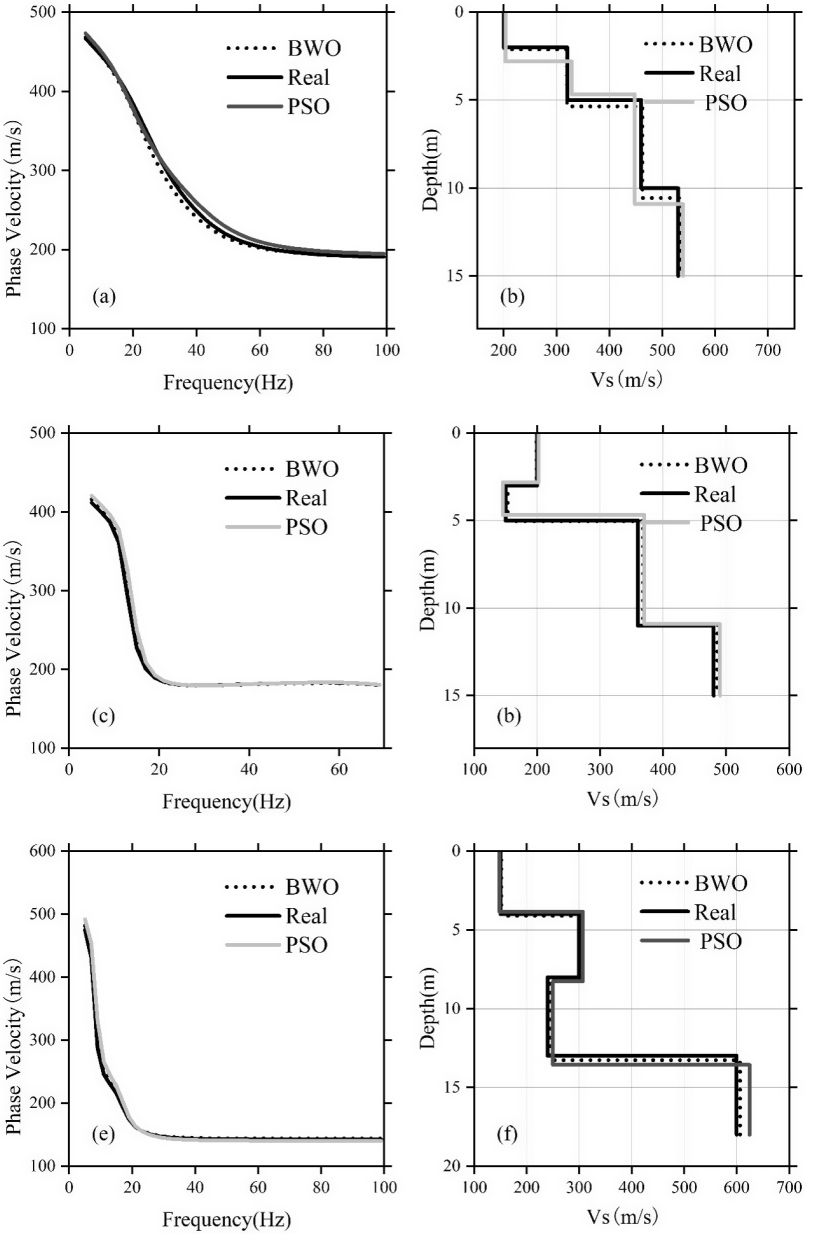


Fig. 3. Inversion results for models B, C, and D: (a, c, e) inverted dispersion curves; (b, d, f) inverted shear-wave velocity profiles.

In the formula, $v_{\text{noise}}$ is the phase velocity after noise addition, $v$ is the phase velocity before noise addition, $r$ is a random number within the range of $(0, 1)$, and $p$ is the degree of noise added with a range of $0-100\%$.

The inversion results of BWO for the noisy models are shown in Figure 4, where subfigures a-h sequentially present the inversion outcomes for models A, B, C, and D. Observing Figures 4b, d, f, h, it is evident that even with the introduction of 15% noise, the model parameters obtained from inversion remain highly consistent with the true model parameters. Specif-

Table 2. Model A, B, C, D: inversion results of BWO for noise-free and noisy data.

| | Model Parameters | True Value | Noise-Free Results | | | | Noisy Results (15%) | | | |
|---|---|---|---|---|---|---|---|---|---|---|
| | | | Mean | Error | RMSE | STD | Mean | Error | RMSE | STD |
| A | $Vs_1$ (m/s) | 200 | 199.24 | 0.38% | 1.26 | 1.28 | 193.69 | 3.16% | 3.39 | 3.51 |
| | $Vs_2$ (m/s) | 450 | 447.40 | 0.58% | 5.94 | 5.98 | 453.78 | 0.84% | 12.16 | 12.52 |
| | $H_1$ (m) | 5 | 4.71 | 5.80% | 0.17 | 0.18 | 5.46 | 9.20% | 0.34 | 0.36 |
| B | $Vs_1$ (m/s) | 200 | 201.21 | 0.61% | 2.39 | 2.52 | 208.12 | 4.06% | 6.44 | 6.73 |
| | $Vs_2$ (m/s) | 320 | 319.87 | 0.04% | 6.97 | 7.42 | 325.28 | 1.65% | 5.32 | 5.6 |
| | $Vs_3$ (m/s) | 460 | 462.23 | 0.48% | 8.87 | 9.34 | 477.83 | 3.88% | 20.46 | 21.47 |
| | $Vs_4$ (m/s) | 530 | 533.52 | 0.66% | 5.72 | 6.03 | 542.12 | 2.29% | 8.16 | 8.5 |
| | $H_1$ (m) | 2 | 2.12 | 6.00% | 0.10 | 0.11 | 2.21 | 10.50% | 0.24 | 0.25 |
| | $H_2$ (m) | 3 | 3.23 | 7.67% | 0.24 | 0.28 | 3.35 | 11.67% | 0.36 | 0.38 |
| | $H_3$ (m) | 5 | 5.21 | 4.20% | 0.49 | 0.53 | 5.11 | 2.20% | 0.24 | 0.25 |
| C | $Vs_1$ (m/s) | 200 | 198.91 | 0.55% | 8.81 | 9.25 | 199.9 | 0.05% | 6.07 | 6.35 |
| | $Vs_2$ (m/s) | 150 | 153.28 | 2.19% | 4.29 | 4.52 | 160.55 | 7.03% | 8.83 | 9.21 |
| | $Vs_3$ (m/s) | 360 | 368.14 | 2.26% | 11.50 | 12.13 | 382.71 | 6.31% | 18.21 | 19.13 |
| | $Vs_4$ (m/s) | 480 | 485.71 | 1.19% | 12.78 | 13.58 | 506.23 | 5.46% | 18.05 | 18.96 |
| | $H_1$ (m) | 3 | 2.91 | 3.00% | 0.16 | 0.17 | 3.26 | 8.67% | 0.35 | 0.37 |
| | $H_2$ (m) | 2 | 2.12 | 6.00% | 0.41 | 0.43 | 2.07 | 3.50% | 0.27 | 0.28 |
| | $H_3$ (m) | 6 | 5.89 | 1.83% | 0.20 | 0.21 | 5.65 | 5.83% | 0.30 | 0.32 |
| D | $Vs_1$ (m/s) | 150 | 151.68 | 1.12% | 0.99 | 1.03 | 149.8 | 0.13% | 6.51 | 6.83 |
| | $Vs_2$ (m/s) | 300 | 302.40 | 0.80% | 4.04 | 4.25 | 283.41 | 5.53% | 8.82 | 9.21 |
| | $Vs_3$ (m/s) | 240 | 245.32 | 2.22% | 3.75 | 3.94 | 261.01 | 8.75% | 22.27 | 23.35 |
| | $Vs_4$ (m/s) | 600 | 606.32 | 1.05% | 4.58 | 4.8 | 620.46 | 3.41% | 3.45 | 3.62 |
| | $H_1$ (m) | 4 | 4.11 | 2.75% | 0.07 | 0.07 | 4.26 | 6.50% | 0.26 | 0.27 |
| | $H_2$ (m) | 4 | 3.98 | 0.50% | 0.13 | 0.14 | 3.78 | 5.50% | 0.17 | 0.18 |
| | $H_3$ (m) | 5 | 5.19 | 3.80% | 0.22 | 0.23 | 5.13 | 2.60% | 0.12 | 0.13 |

ically, the maximum relative errors for parameters inverted by BWO for models A, B, C, and D are 9.20%, 11.67%, 8.67%, and 8.75%, respectively (detailed in Table 2). Compared to the results from noise-free models (A, B, C, D max relative errors: 5.80%, 7.67%, 6.00%, 3.80%), the parameter differences are within acceptable limits. In summary, although noise affects the inversion results to some extent, BWO can still achieve good inversion results when inverting dispersion curves with 15% noise, and its inversion performance is better than that of PSO. This indicates that BWO possesses

Table 3. Model A, B, C, D: inversion results of PSO for noise-free and noisy data.

| | Model Parameters | True Value | Noise-Free Results | | | | Noisy Results (15%) | | | |
|---|---|---|---|---|---|---|---|---|---|---|
| | | | Mean | Error | RMSE | STD | Mean | Error | RMSE | STD |
| A | $Vs_1$ (m/s) | 200 | 195.59 | 2.20% | 5.15 | 5.43 | 187.31 | 6.35% | 8.96 | 9.43 |
| | $Vs_2$ (m/s) | 450 | 443.32 | 1.48% | 7.64 | 8.10 | 476.02 | 5.78% | 17.32 | 18.31 |
| | $H_1$ (m) | 5 | 4.58 | 8.40% | 0.29 | 0.31 | 4.51 | 9.80% | 0.58 | 0.61 |
| B | $Vs_1$ (m/s) | 200 | 203.73 | 1.87% | 3.91 | 4.13 | 209.73 | 4.87% | 9.60 | 10.12 |
| | $Vs_2$ (m/s) | 320 | 329.22 | 2.88% | 9.59 | 10.11 | 314.22 | 1.81% | 20.50 | 21.61 |
| | $Vs_3$ (m/s) | 460 | 448.15 | 2.58% | 6.75 | 7.12 | 485.15 | 5.47% | 16.35 | 17.23 |
| | $Vs_4$ (m/s) | 530 | 539.11 | 1.72% | 10.67 | 11.25 | 551.11 | 3.98% | 16.00 | 16.85 |
| | $H_1$ (m) | 2 | 1.96 | 2.00% | 0.32 | 0.34 | 1.93 | 3.50% | 0.39 | 0.41 |
| | $H_2$ (m) | 3 | 3.31 | 10.33% | 0.28 | 0.30 | 3.35 | 11.67% | 0.30 | 0.32 |
| | $H_3$ (m) | 5 | 4.81 | 3.80% | 0.77 | 0.81 | 4.76 | 4.80% | 0.50 | 0.53 |
| C | $Vs_1$ (m/s) | 200 | 210.03 | 5.02% | 17.29 | 18.37 | 185.27 | 7.37% | 10.96 | 11.55 |
| | $Vs_2$ (m/s) | 150 | 145.54 | 2.97% | 2.99 | 3.18 | 175.13 | 16.75% | 16.20 | 17.18 |
| | $Vs_3$ (m/s) | 360 | 372.34 | 3.43% | 18.13 | 19.28 | 347.28 | 3.53% | 12.58 | 13.26 |
| | $Vs_4$ (m/s) | 480 | 491.34 | 2.36% | 22.68 | 24.14 | 514.19 | 7.12% | 25.91 | 27.31 |
| | $H_1$ (m) | 3 | 2.81 | 6.33% | 0.26 | 0.27 | 3.35 | 11.67% | 0.47 | 0.49 |
| | $H_2$ (m) | 2 | 1.87 | 6.50% | 0.58 | 0.61 | 2.27 | 13.50% | 0.20 | 0.21 |
| | $H_3$ (m) | 6 | 6.21 | 3.50% | 0.16 | 0.17 | 6.41 | 6.83% | 0.54 | 0.57 |
| D | $Vs_1$ (m/s) | 150 | 147.71 | 1.53% | 11.5 | 12.12 | 152.14 | 1.43% | 13.21 | 13.92 |
| | $Vs_2$ (m/s) | 300 | 307.21 | 2.40% | 20.04 | 21.12 | 329.12 | 9.71% | 20.25 | 21.34 |
| | $Vs_3$ (m/s) | 240 | 250.31 | 4.30% | 27.24 | 28.71 | 268.19 | 11.75% | 30.30 | 31.93 |
| | $Vs_4$ (m/s) | 600 | 624.54 | 4.09% | 20.23 | 21.32 | 632.35 | 5.39% | 12.06 | 12.71 |
| | $H_1$ (m) | 4 | 3.85 | 3.75% | 0.24 | 0.25 | 4.30 | 7.50% | 0.32 | 0.34 |
| | $H_2$ (m) | 4 | 4.41 | 10.25% | 0.64 | 0.68 | 3.67 | 8.25% | 0.24 | 0.26 |
| | $H_3$ (m) | 5 | 5.32 | 6.40% | 0.87 | 0.92 | 5.27 | 5.40% | 0.27 | 0.29 |

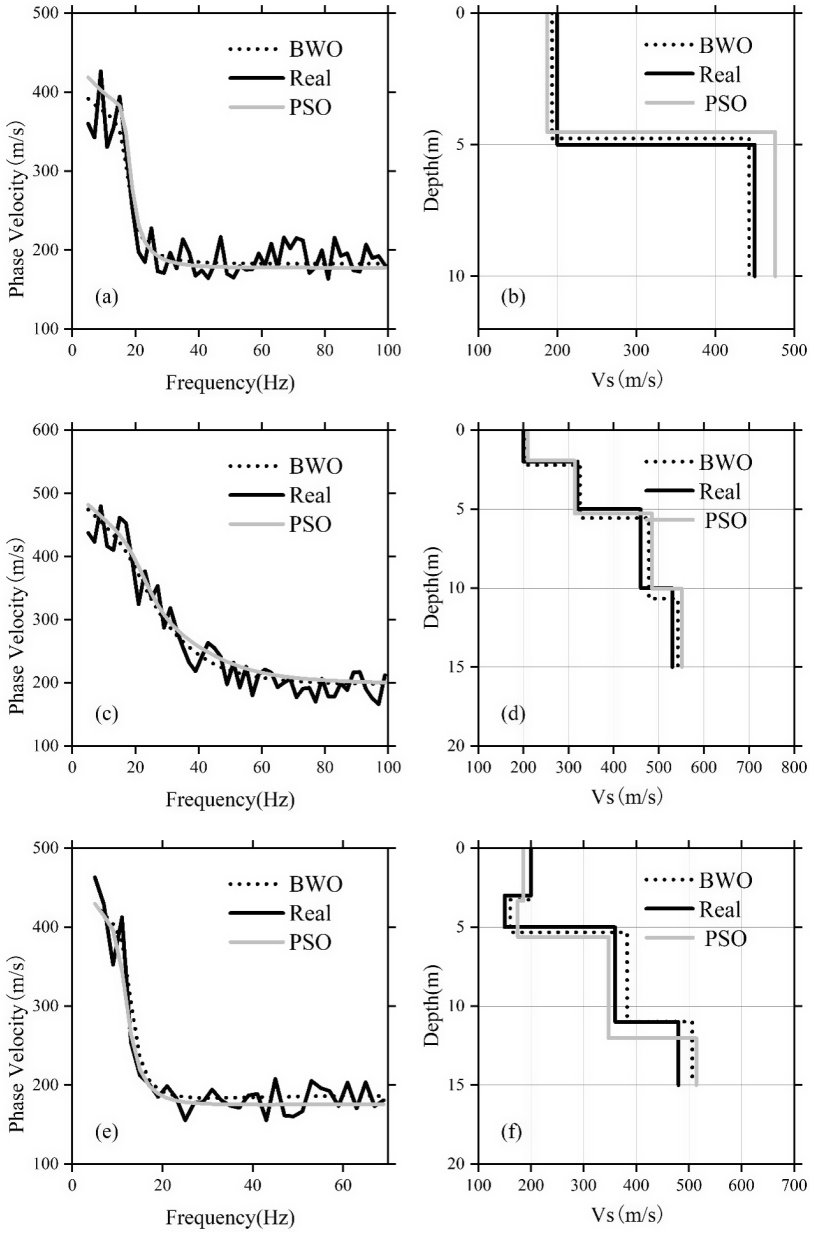


Fig. 4. Inversion results for noisy data from models A, B, C, D: (a, c, e, g) inverted dispersion curves; (b, d, f, h) inverted shear-wave velocity profiles. See next page.

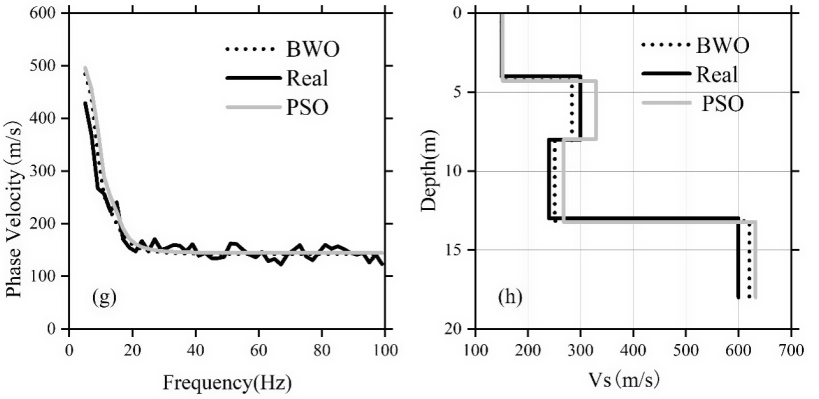


Fig. 4. Continuation from the previous page.

strong anti-noise performance, is superior to the PSO algorithm in both inversion accuracy and anti-noise capability, and is suitable for handling data inversion tasks with strong noise.

### 3.3. Multi-mode dispersion curve inversion

In some special subsurface conditions (e.g., soft interlayers), higher-mode waves may exhibit stronger energy than the fundamental mode in the high-frequency part. In such cases, jointly inverting higher-mode dispersion curves with the fundamental-mode curve can increase the effective information for inversion, thereby improving the accuracy of the obtained stratigraphic information. Therefore, testing the algorithm's ability to invert multi-mode dispersion curves is necessary. This test used model C as an example, adding higher-mode data to its fundamental-mode dispersion curve data for inversion. The inversion results are shown in Fig. 5 and Table 4. Figure 5a shows that the inverted dispersion curves (dotted lines), whether fundamental or higher-mode, fit the true model dispersion curves (solid lines) very well. Figure 5b indicates that the inverted model parameters (dotted line) also differ only slightly from the true model parameters (solid line), demonstrating the feasibility of using BWO for multi-mode dispersion curve inversion. Comparison of the inversion results for BWO and PSO reveals that both algorithms achieve excellent fitting to the true values for the fundamental-mode dispersion curves they invert. However, the

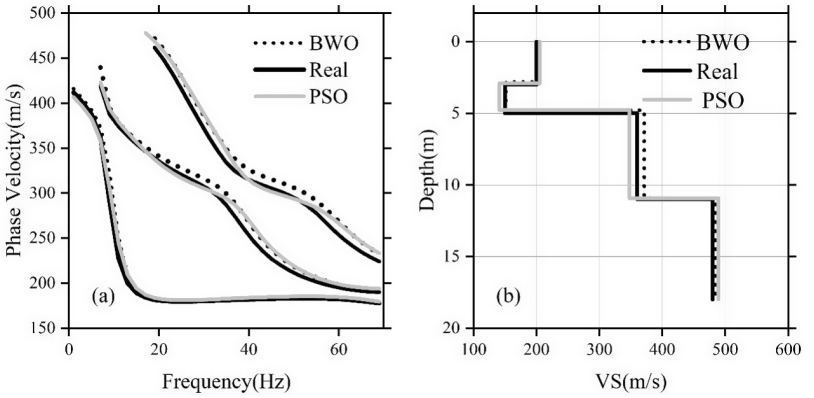


Fig. 5. Multi-mode data inversion results for model C: (a) inverted dispersion curves; (b) inverted shear-wave velocity profile. The raw seismic records are shown in Fig. 7a. The seismic records were imported into the code and then converted into a dispersion energy map. And Figure 7b presents the converted dispersion energy map.

first-mode and second-mode dispersion curves inverted by PSO exhibit a substantial deviation from the true values. This observation demonstrates that BWO is also superior to PSO in addressing multi-mode dispersion inversion problems. Furthermore, the accuracy of the multi-mode inversion results generally improved compared to using only the fundamental mode. This indicates that multi-mode dispersion curve inversion yields more accurate model parameters and superior inversion effectiveness compared to inversion using only the fundamental-mode dispersion curve.

Table 4. Model C: inversion results of multi-mode data for BWO and PSO.

| Parameter | True Value | Noise-Free Results | | | | Noisy Results (15%) | | | |
|---|---|---|---|---|---|---|---|---|---|
| | | Mean | Error | RMSE | STD | Mean | Error | RMSE | STD |
| $Vs_1$ (m/s) | 200 | 200.12 | 0.06% | 9.69 | 10.21 | 205.34 | 2.67% | 14.43 | 15.21 |
| $Vs_2$ (m/s) | 150 | 151.48 | 1.00% | 3.10 | 3.27 | 141.25 | 5.83% | 9.71 | 10.23 |
| $Vs_3$ (m/s) | 360 | 371.08 | 3.08% | 10.48 | 11.04 | 347.79 | 3.39% | 8.94 | 9.42 |
| $Vs_4$ (m/s) | 480 | 484.21 | 0.88% | 14.54 | 15.32 | 489.29 | 1.94% | 27.87 | 29.38 |
| $H_1$ (m) | 3 | 2.82 | 6.00% | 0.10 | 0.11 | 2.89 | 3.67% | 0.07 | 0.08 |
| $H_2$ (m) | 2 | 1.97 | 1.50% | 0.46 | 0.48 | 1.87 | 6.50% | 0.58 | 0.61 |
| $H_3$ (m) | 6 | 6.11 | 1.83% | 0.17 | 0.18 | 6.16 | 2.67% | 0.30 | 0.32 |

## 4. Comparison with particle swarm optimization

To verify the effectiveness of the BWO algorithm in obtaining accurate subsurface parameters through dispersion curve inversion, this study compared it with the classic Particle Swarm Optimization (PSO) algorithm. The systematic comparison, analysis, and evaluation aimed to reveal the inversion efficiency of both algorithms. The test selected the noise-free model D. During inversion, the population size, search space, and iteration count were kept consistent for both algorithms: population size was set to 30, iteration count to 100, matching the settings used earlier (PSO algorithm parameters configured according to *Fu et al. (2022)*.

The inversion results are shown in Figure 6, with specific inversion parameters detailed in Table 4. Figure 6a shows that both algorithms can fit

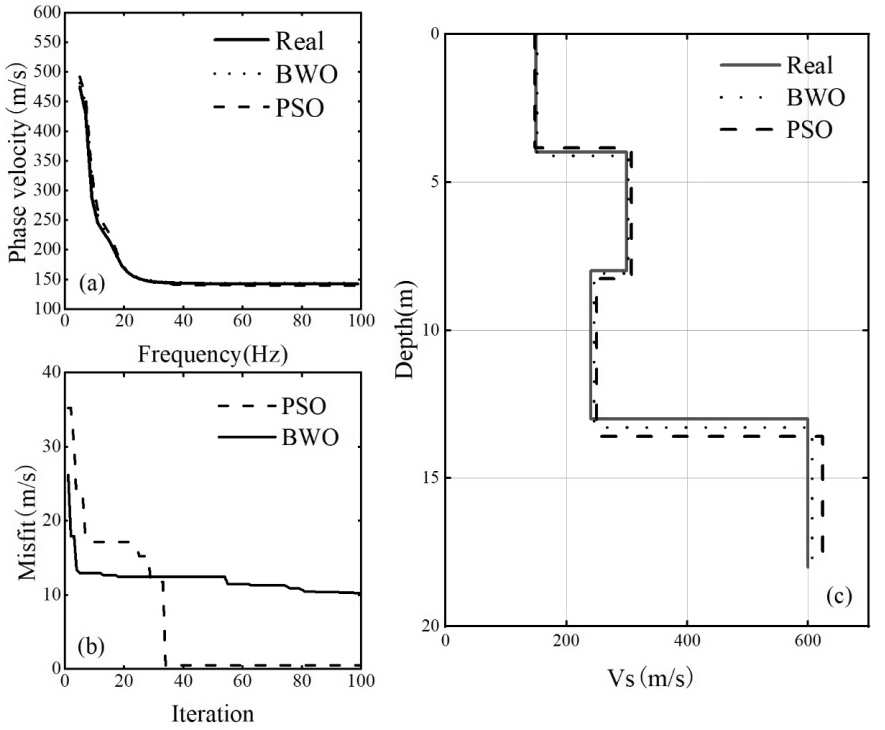


Fig. 6. BWO and PSO inversion results for noise-free model D: (a) inverted dispersion curves; (b) minimum objective function value vs. iteration count; (c) comparison of inverted shear-wave velocity profiles.

the dispersion curve well, achieving a high degree of fit. However, Figure 6c clearly shows that BWO outperforms PSO in reconstructing the thickness and shear-wave velocity of the fourth layer. Moreover, from the iteration process in Figure 6b, BWO converges rapidly towards the optimal solution within about 30 iterations, while PSO still shows a trend of moving towards the optimum even after 100 iterations. At iteration 100, BWO's misfit value is significantly lower than PSO's. Additionally, comparing the standard deviations of the inversion results for each model parameter in Table 4 reveals that the stability of the BWO algorithm is significantly better than that of the traditional PSO algorithm.

In conclusion, for the Rayleigh wave dispersion curve inversion problem, the BWO algorithm, compared to the PSO algorithm, offers higher inversion accuracy, faster convergence speed, and stronger stability.

## 5. Field data test

The test results from the aforementioned theoretical models clearly demonstrate the feasibility and effectiveness of applying the BWO algorithm to dispersion curve inversion. To validate its applicability for real-world data inversion, this study used measured data from Wyoming, USA (data sourced from *Xia, 2014*) for testing. During data acquisition, a hammer impact source was used for excitation, with 48 channels of vertical geophones employed for signal reception. The minimum shot interval and geophone interval were both set to 0.9 metres.

The raw seismic records are shown in Fig. 7a. The seismic records were imported into the code and then converted into a dispersion energy map. Figure 7b presents the converted dispersion energy map. Due to the presence of mode merging phenomenon in high-mode data, extracting high-mode dispersion curves may lead to misjudgement, which in turn results in inversion errors. Therefore, the fundamental-mode dispersion curve was manually picked based on energy intensity for inversion. The frequency band range used for inversion is $10-30$ Hz. The algorithm parameters were set consistent with the previous theoretical model tests. The inverted model parameters are shown in Table 5.

The inversion results are shown in Figure 8. Analysis of Figures 8a and 8b reveals that the inverted dispersion curve (solid line in Fig. 8a) achieves

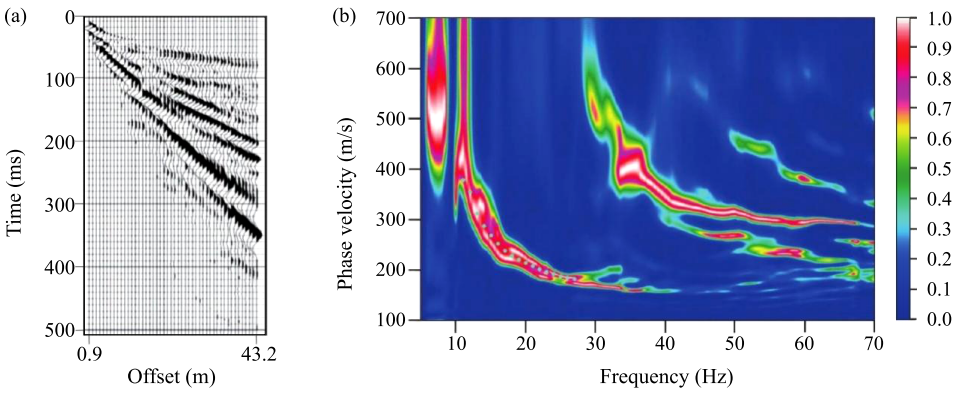


Fig. 7. Field data in Wyoming (a) and its dispersion image (b) (*Xia, 2014*).

a high degree of fit with the measured data dispersion curve (dotted line in Fig. 8a). The inversion process converged within just over 20 iterations. In the shallow subsurface (within 10 m), the shear-wave velocity model reconstructed by BWO (solid line in Fig. 8c) shows high agreement with borehole data (diamond-marked polyline in Fig. 8c). Beyond 10m depth, the reconstructed model still follows the borehole data well and aligns with the trend of previous inversion results. This result fully demonstrates the high reliability of BWO when applied to real-world data inversion.

Table 5. Inversion model and search range for field data (*Cai et al., 2018b*).

| Layers | *Vs* (m/s) | *h* (m) | Poisson's Ratio | $\rho$ (g/cm) |
|---|---|---|---|---|
| 1 | $100 \sim 300$ | $1 \sim 5$ | 0.38 | 2.0 |
| 2 | $100 \sim 400$ | $1 \sim 5$ | 0.38 | 2.0 |
| 3 | $100 \sim 600$ | $1 \sim 5$ | 0.35 | 2.0 |
| 4 | $200 \sim 600$ | $1 \sim 5$ | 0.35 | 2.0 |
| 5 | $200 \sim 800$ | $\infty$ | 0.30 | 2.0 |

## 6. Conclusion

This study introduces a novel swarm intelligence optimization algorithm—Beluga Whale Optimization (BWO)—into the field of Rayleigh wave dispersion curve inversion. In terms of inversion strategy design, broad model

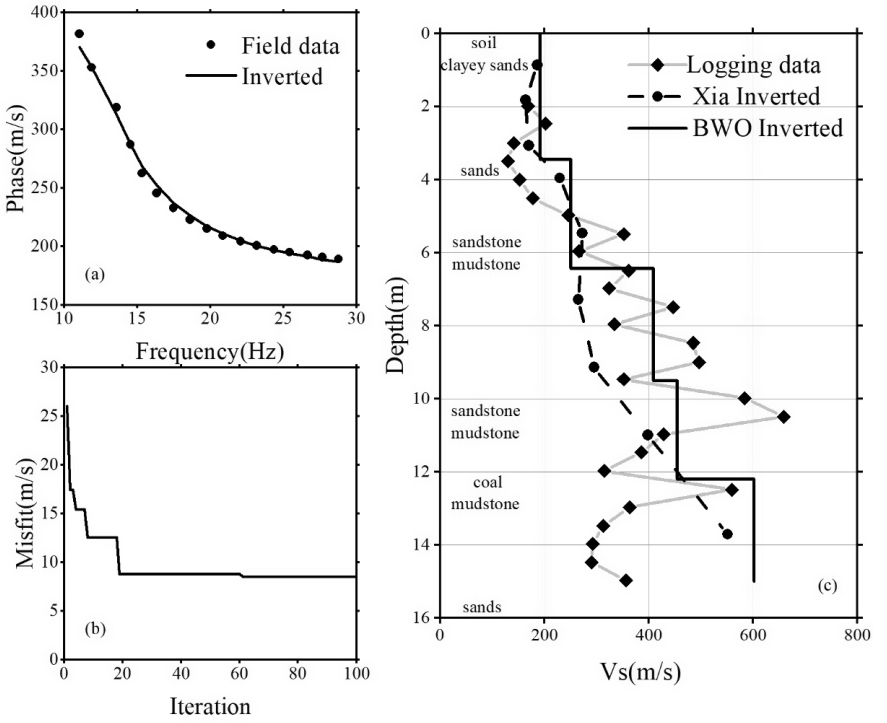


Fig. 8. Field data dispersion curve inversion results: (a) inverted dispersion curve; (b) minimum objective function value vs. iteration count; (c) reconstructed shear-wave velocity result.

parameter search spaces (layer thickness, shear-wave velocity) were set to simulate complex exploration scenarios lacking prior information, better aligning with practical application needs. To systematically verify the applicability of BWO: (1) Multiple theoretical models were constructed (covering simple-complex structures, noise-free-noisy data) to comprehensively evaluate algorithm performance; (2) Measured data from Wyoming, USA, was used to test its real-world application performance. The test results indicate:

(1) BWO demonstrates strong exploration and exploitation capabilities in the solution space. It achieves high-accuracy subsurface parameter inversion while possessing fast convergence and strong robustness, highlighting its potential for application in geophysical inversion.

(2) Compared to the traditional Particle Swarm Optimization algorithm, BWO exhibits higher accuracy, faster convergence speed, and stronger stability in Rayleigh wave dispersion curve inversion.

***Author contributions***. All authors have contributed to the conceptualization of this research and computer implementation of the methods. All authors have read and agreed to the published version of the manuscript.

***Conflict of interest***. The authors state no conflicts of interest relevant to this study.

***Acknowledgements***. We are very grateful to Dr. Peter Vajda and two anonymous reviewers for their constructive comments and suggestions that have improved the quality of the paper.

***Funding***. The author(s) declare that financial support was received for the research, authorship, and/or publication of this article. This study was funded by the Nanchang Normal University 2025 University-Level Scientific Research Projects (grant number: 25XJZR02).

## References

Ai D., Cheng Q., 2009: Estimation of 2D s-wave velocity section with low velocity layers by OCCAM algorithm. Geotech. Investig. Surv., **37**, 4, 87–90.

Ai H., Li H., Song X., Li T., Su K., Chen H., Fu Y., Mei Z., 2025: Global and full-parametric optimization of multi-mode Rayleigh wave dispersion curves for estimating glacial ice structure. Chin. J. Geophys., **68**, 6, 2320–2347, doi: 10.6038/cjg2024R0349 (in Chinese).

Arai H., Tokimatsu K., 2005: S-wave velocity profiling by joint inversion of microtremor dispersion curve and horizontal-to-vertical (H/V) spectrum. Bull. Seismol. Soc. Am., **95**, 5, 1766–1778, doi: 10.1785/0120040243.

Beaty K S., Schmitt D R., Sacchi M., 2002: Simulated annealing inversion of multimode Rayleigh wave dispersion curves for geological structure. Geophys. J. Int., **151**, 2, 622–631, doi: 10.1046/j.1365-246X.2002.01809.x.

Cai W., Song X., Yuan S., Hu Y., 2018a: Fast and stable Rayleigh-wave dispersion-curve inversion based on particle swarm optimization. Oil Geophys. Prospect., **53**, 1, 25–34 + 4–5, doi: 10.13810/j.cnki.issn.1000-7210.2018.01.004.

Cai W., Song X., Yuan S., Hu Y., 2018b: Inversion of Rayleigh wave dispersion curves based on firefly and bat algorithms. Chin. J. Geophys., **61**, 6, 2409–2420, doi: 10.6038/cjg2018L0322 (in Chinese).

Calderón-Macías C., Luke B., 2007: Improved parameterization to invert Rayleigh-wave data for shallow profiles containing stiff inclusions. Geophysics, **72**, 1, U1–U10, doi: 10.1190/1.2374854.

Dal Moro G., Pipan M., Gabrielli P., 2007: Rayleigh wave dispersion curve inversion via genetic algorithms and marginal posterior probability density estimation. J. Appl. Geophys., **61**, 1, 39–55, doi: 10.1016/j.jappgeo.2006.04.002.

Dal Moro G., Moustafa S. S. R., Al-Arifi N. S., 2018: Improved Holistic Analysis of Rayleigh Waves for Single- and Multi-Offset Data: Joint Inversion of Rayleigh-Wave Particle Motion and Vertical- and Radial-Component Velocity Spectra. Pure Appl. Geophys., **175**, 1, 67–88, doi: 10.1007/s00024-017-1694-8.

Dorman J., Ewing M., 1962: Numerical inversion of seismic surface wave dispersion data and crust-mantle structure in the New York-Pennsylvania area. J. Geophys. Res., **67**, 13, 5227–5241, doi: 10.1029/JZ067i013p05227.

Fu Y., Yang A., Yao Z., Liu Y., Li H., Chen H., Wang X., 2022: Inversion of Rayleigh Wave Dispersion Curves via Long Short-Term Memory Combined with Particle Swarm Optimization. Comput. Intell. Neurosci., **2022**, 1, 2640929, doi: 10.1155/2022/2640929.

Fu Y. Ai H., Yao Z., Mei Z., Su K., 2023a: Inversion of the Rayleigh wave dispersion curves based on the sine-cosine algorithm. Geophys. Geochem. Explor., **47**, 6, 1467–1478, doi: 10.11720/wtyht.2023.1239 (in Chinese with English abstract).

Fu Y., Ai H., Yao Z., Li H., Tian X., Zhang X., 2023b: Inversion of multi-mode Rayleigh wave dispersion curves based on lightning attachment procedure optimization. Oil Geophys. Prospect., **58**, 4, 830–838, doi: 10.13810/j.cnki.issn.1000-7210.2023.04.008 (in Chinese with English abstract).

Gabriels P., Snieder R., Nolet G., 1987: In situ measurements of shear-wave velocity in sediments with higher-mode Rayleigh waves. Geophys. Prospect., **35**, 2, 187–196, doi: 10.1111/j.1365-2478.1987.tb00812.x.

Ganji V., Gucunski N., Nazarian S. 1998: Automated inversion procedure for spectral analysis of surface waves. J. Geotech. Geoenviron. Eng., **124**, 8, 757–770, doi: 10.1061/(ASCE)1090-0241(1998)124:8(757).

Lamuraglia S., Stucchi E., Aleardi M., 2023: Application of a global–local full-waveform inversion of Rayleigh wave to estimate the near-surface shear wave velocity model. Near Surf. Geophys., **21**, 1, 21–38, doi: 10.1002/nsg.12243.

Liu Z., Li J., Hanafy S. M., Schuster G., 2018: 3D wave-equation dispersion inversion of Rayleigh waves. Geophysics, **84**, 5, R673–R691, doi: 10.1190/geo2018-0543.1.

Liu X., Lü X., Shao Y., Chen C., Liu G., Li Y., Li M., Wu X., Chen Y., 2024: Monitoring and disaster prevention of high and steep sandstone slopes along highways under construction. Front. Earth Sci., **12**, 1444592, doi: 10.3389/feart.2024.1444592.

Lu Y., Peng S., Du W., Zhang X., Ma Z., Lin P., 2016: Rayleigh wave inversion using heat-bath simulated annealing algorithm. J. Appl. Geophys., **134**, 267–280, doi: 10.1016/j.jappgeo.2016.09.008.

Martınez M. D., Lana X., Olarte J., Badal J., Canas J. A., 2000: Inversion of Rayleigh wave phase and group velocities by simulated annealing. Phys. Earth Planet. Inter., **122**, 1-2, 3–17, doi: 10.1016/S0031-9201(00)00183-7.

Nong X., Wang Y., Lin B., Xu W., Luo W., Tang R., 2024: Performance of Diaphragm Walls during Ultra-Deep Excavations in Karst Areas: Field Monitoring Analysis. Adv. Civ. Eng., **2024**, 5834253, doi: 10.1155/2024/5834253.

Pei D., Louie J N., Pullammanappallil S K., 2007: Application of simulated annealing inversion on high-frequency fundamental-mode Rayleigh wave dispersion curves. Geophysics, **72**, 5, R77–R85, doi: 10.1190/1.2752529.

Pei J., Wu Y., Liu Y., 1994: Near Surface Low Velocity Zone Inversion. J. Jilin Univ., **3**, 317–320 + 326, doi: 10.13278/j.cnki.jjuese.1994.03.014.

Shi Y., Jin W., 1995: Gentic Algorithms Inversion of Lithospheric Structure from Surface wave Dispersion. Chin. J. Geophys., **38**, 2, 189–198 (in Chinese with English abstract).

Song X., Xiao B., Huang R., Gu H., Zhang X., 2003: The inversion of dispersion curves using self-adaptively iterative damping least square method by combining equal thinner layers with weighting matrix. Geophys. Geochem. Explor., **27**, 3, 212–216 (in Chinese).

Song X., Gu H., Liu J., Zhang X., 2007: Estimation of shallow subsurface shear-wave velocity by inverting fundamental and higher-mode Rayleigh waves. Soil Dyn. Earthq. Eng., **27**, 7, 599–607, doi: 10.1016/j.soildyn.2006.12.003.

Song X., Tang L., Lv X., Fang H., Gu H., 2012: Application of particle swarm optimization to interpret Rayleigh wave dispersion curves. J. Appl. Geophys., **84**, 1–13, doi: 10.1016/j.jappgeo.2012.05.011.

Wang C., Shi Z., Yang W., Wei Y., Huang M., 2022: High-resolution shallow anomaly characterization using cross-hole P- and S-wave tomography. J. Appl. Geophys., **201**, 104649, doi: 10.1016/j.jappgeo.2022.104649.

Xia J., 2014: Estimation of near-surface shear-wave velocities and quality factors using multichannel analysis of surface-wave methods. J. Appl. Geophys., **103**, 140–151, doi: 10.1016/j.jappgeo.2014.01.016.

Xia J., Miller R. D., Park C. B., 1999: Estimation of near-surface shear-wave velocity by inversion of Rayleigh waves. Geophysics, **64**, 3, 691–700, doi: 10.1190/1.1444578.

Yamanaka H., Ishida H., 1996: Application of genetic algorithms to an inversion of surface-wave dispersion data. Bull. Seismol. Soc. Am., **86**, 2, 436–444, doi: 10.1785/BSSA0860020436.

Yang B., Xiong Z., Zhang D., Yang Z., 2019: Rayleigh surface-wave dispersion curve inversion based on adaptive chaos genetic particle swarm optimization algorithm. Oil Geophys. Prospect., **54**, 6, 1217–1227 + 1172, doi: 10.13810/j.cnki.issn.1000-7210.2019.06.005.

Yang X., Han P., Yang Z., Chen X., 2023: Two-stage broad learning inversion framework for shear-wave velocity estimation. Geophysics, **88**, 1, WA219–WA237, doi: 10.1190/geo2022-0060.1.

Zeng C., Xia J., Miller R. D., Tsoflias G. P., 2011: Feasibility of waveform inversion of Rayleigh waves for shallow shear-wave velocity using a genetic algorithm. J. Appl. Geophys., **75**, 4, 648–655, doi: 10.1016/j.jappgeo.2011.09.028.

Zhang B., Xiao B., Yang W., Cao S., Mou Y., 2000: Study on mechanism and inversion of zigzag dispersion curves in Rayleigh wave exploration. Chin. J. Geophys., **43**, 4, 591–601, doi: 10.1002/cjg2.73.

Zhang C., Wu C., Wang P., 2020: Seismic Fragility Analysis of Bridge Group Pile Foundations considering Fluid-Pile-Soil Interaction. Shock Vib., **2020**, 838813, doi: 10.1155/2020/8838813.

Zhong C., Li G., Meng Z., 2022: Beluga whale optimization: A novel nature-inspired metaheuristic algorithm. Knowl. Based Syst., **251**, 109215, doi: 10.1016/j.knosys.2022.109215.